

Temperature-dependent tunneling spectra of $\text{Bi}_2\text{Sr}_2\text{CaCu}_2\text{O}_8$ single crystals with well-defined $\text{Bi}_2\text{Sr}_2\text{CuO}_6$ epitaxial layers

Takuya Matsumoto, Supab Choopun, and Tomoji Kawai

Institute of Scientific and Industrial Research, Osaka University, Mihogaoka, Ibaraki, Osaka 567, Japan

(Received 18 October 1994)

The temperature dependence of the tunneling conductance $G(V, T)$ along the c axis of $\text{Bi}_2\text{Sr}_2\text{CaCu}_2\text{O}_8$ single crystals has been investigated using epitaxial junctions of the type $\text{Au}/\text{Bi}_2\text{Sr}_2\text{CuO}_6$ thin-film layer/ $\text{Bi}_2\text{Sr}_2\text{CaCu}_2\text{O}_8$ single crystal. A linear background conductance is observed, which appears to originate from a normal density-of-states effect. The background can be adequately described by a simple first-order relation using only one fitting parameter. The shape of the superconducting gap agrees well with a convolution of this linear background and a BCS-like density of states that includes Andreev reflection. The fits yield values for the ratio $2\Delta(T=11\text{ K})/k_B T_c$ (84 K) = 5.4–6.0 and a very small lifetime width $\Gamma(T=11\text{ K}) < 0.1\text{ meV}$. The data suggest that the zero-bias conductance is intrinsically low or zero, suggesting an s -like character for the superconducting pairing function along the c axis in $\text{Bi}_2\text{Sr}_2\text{CaCu}_2\text{O}_8$.

I. INTRODUCTION

Electron tunneling is the most direct method for study of the density of states (DOS) near the Fermi surface.¹ Historically, tunneling measurements have provided detailed information concerning the superconductivity mechanism and experimental evidence for the BCS model.² Considerable efforts have been expended on tunneling investigations of the high- T_c superconductors (HTSC's). For cubic $\text{Ba}_{1-x}\text{K}_x\text{BiO}_3$, a BCS-like DOS with $2\Delta/k_B T_c = 3.8$ – 3.9 has been obtained.^{3–5} In the case of the cuprate HTSC materials, however, the nature of the gap has been quite controversial as reported in an exhaustive discussion of the current status by Kirtley.⁶ Typically, the spectra contain various anomalies such as a high zero-bias conductance, a zero-bias conductance peak (ZBCP), a linear (V-shaped) background, a broad gap, and large conductance peaks at the gap edge. These features deviate substantially from those of BCS superconductors, and they are important with respect to the superconductivity mechanism of HTSC's. Especially, the structure inside the gap relates to the symmetry of the electron pairing wave function. These spectral shapes, however, may not directly reflect the superconducting DOS because of the following two difficulties.

First, the tunneling spectra of HTSC's often exhibit a conductance background which increases linearly with the voltage and which depends strongly on the temperature.^{7–13} This background complicates evaluation of the true superconducting gap shape. For HTSC's, it is difficult to obtain the normal-state background spectrum at $T < T_c$ because the superconducting gap cannot be eliminated by available magnetic fields. Accordingly, the background should be derived from a systematic analysis of its temperature dependence above T_c . Furthermore, the proper way to deconvolute the superconducting DOS from the background has not yet been established because the origin of the background conductance is unclear. This deconvolution should be consistent with a

systematic fitting of the gap structure, including the temperature dependence.

Second, the tunneling studies reported thus far have produced widely scattered results, indicating a range of DOS functions. This seems to be mainly due to the fact that the interface with HTSC's easily degrades during the fabrication process of the insulating junction layer.¹⁴ Since HTSC's typically have extremely short coherence lengths, this means that the tunneling spectra reflect the DOS of the degraded region near the junction interface. Thus a sharp interface with superconducting properties that remain intact up to the interface is of the utmost importance for reliable measurements.

Tunneling measurements on the $\text{Bi}_2\text{Sr}_2\text{CaCu}_2\text{O}_8$ compound have been reported in the literature using break junctions,^{9,15,16} point contacts,^{10,11,17–19} scanning tunneling microscopy^{12,13,20–24} (STM), and planar tunnel junctions on films and single crystals.^{25–28} Most data were obtained with the point-contact and break-junction techniques. With these methods, however, it is difficult to perform well-characterized tunneling spectroscopy because the nature of the interface and tunneling barrier generally is unknown. Furthermore, these techniques lack the stability to perform quantitative temperature-dependent tunneling measurements. In STM, electron tunneling occurs through a well-defined vacuum barrier. This technique too, however, cannot be used at different temperatures. Planar junctions provide the only geometry that is stable enough for quantitative studies of the temperature dependence of the tunneling spectra. In spite of these advantages, satisfactory data, especially along the c -axis direction, have been lacking. This is because planar junctions prepared by conventional methods, in many cases, present problems in the form of pin holes or degradation of the superconductivity near the interface. These difficulties, however, can be overcome by using epitaxial tunneling junctions fabricated by laser-molecular-beam epitaxy,²⁹ which has enabled us to obtain reproducible and reliable tunneling spectra.

We have fabricated reliable tunneling junctions of Au/Bi₂Sr₂CuO₆ (2201) thin-film layer/Bi₂Sr₂CaCu₂O₈ (2212) single crystals. The crystal growth of the 2201 film on the 2212 single crystal is expected to be pseudohomoepitaxial because the lattice constants along the in-plane *a* and *b* axes of both compounds are equal. For this reason, this combination of materials is suitable for the fabrication of a well-defined and damage-free interface along the *c*-axis direction.³⁰ Using this junction, we have reported BCS-like tunneling spectra which contain sharp gap edges, low zero-bias conductance, and symmetry with respect to the bias polarity.^{31,32} These spectra can be fitted using a lifetime smearing model and background curves approximated by a polynomial at each temperature.³² However, the temperature dependence of the conductance curve has not been well understood because the lack of an obvious function describing the normal-state (background) conductance in the fitting procedure severely complicated the analysis of the temperature-dependent tunneling spectra.

In this paper, we have obtained reproducible and reliable tunneling spectra over a wide temperature range, which enabled us to systematically analyze the temperature dependence of both the background conductance and the gap structure. We found that the origin of the linear background conductance stems from the normal-state electrical properties of the superconductor material. The gap structure is accurately fitted within the BCS framework including Andreev reflection.

II. EXPERIMENTAL DETAILS

The detailed composition of the tunneling junction Au/2201 barrier/2212 single crystal is shown in Fig. 1. The superconducting 2212 single crystal was grown by a traveling-solvent floating-zone method.³³ The cleaved surface of this crystal is as large as 5 × 10 mm², consisting of a single grain whose topmost atomic layer is BiO based on high-resolution transmission electron microscopy. The 2201 epitaxial layer with a thickness of 20–30 nm was grown on this 2212 crystal by the laser-molecular-beam epitaxy method.²⁹ The reflection high-energy electron-diffraction (RHEED) patterns remained streaky

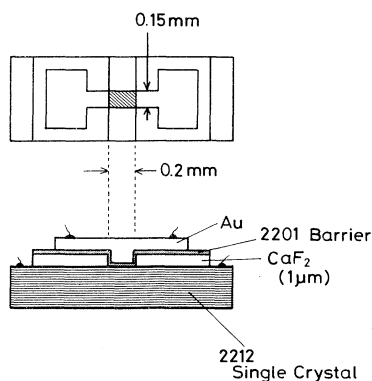


FIG. 1. Schematic composition of the Au/Bi₂Sr₂CuO₆ film layer/Bi₂Sr₂CaCu₂O₈ single-crystal junction. The tunneling region is the crossed area of 0.15 × 0.2 mm².

all during the growth of the 2201 film. In addition, the RHEED intensity oscillated with a period corresponding to 1.2 nm thickness of the 2201 half unit cell. These observations suggest that the 2201 film grows as a flat layer in a layer-by-layer growth mode and that the thickness of the 2201 barrier layer can be controlled by counting the number of RHEED oscillations. In this manner, we have obtained sharp and well-defined 2201/2212 interfaces. Details of the 2201 film growth on 2212 single crystals have already been reported.³⁰

In spite of the good structural stability of the 2212 single crystal under the film growth conditions, we have found that the superconducting properties degrade owing to an oxygen deficiency incurred during the 2201 film growth. Full recovery of the superconducting properties can be induced by annealing the sample in an O₂ atmosphere without destruction of the junction structure. The resistivity-temperature curve of a 2212 single crystal after annealing in O₂ at 650 °C for 3 h shows good metallic behavior in the normal state and yields the superconductive transition *T*_{c0} at 84 K.

The CaF₂ insulating buffer layer and the Au electrode were deposited by conventional evaporation. In order to avoid Au diffusion, the Au electrode is deposited after an anneal of the 2201/2212 junction. The tunneling region has an area of 0.15 mm × 0.2 mm as shown in Fig. 1. The junction resistance is typically several times 10 Ω at room temperature, corresponding to a resistivity of 10³ Ω cm, which is consistent with values obtained for 2201 films on SrTiO₃ substrates.

The tunneling conductance was measured by a conventional four-terminal technique. The conductance curves were recorded on *x-y* charts at a series of temperatures and were later digitized on a 1-mV mesh for fitting with the calculated curves.

III. DATA AND ANALYSIS

The observed tunneling conductance $G_{\text{obs}}(V, T)$, where *V* is the bias voltage and *T* is the temperature, was measured for more than 20 junctions. In these junctions, the superconducting gap structure was observed for 60% of the samples. The spectra for various samples can be classified into two groups depending on the value of zero-bias conductance. Spectra indicating a zero-bias conductance larger than 20% of $G_{\text{obs}}(V=100 \text{ mV}, T)$ at low temperature typically show various anomalies in the gap structure, such as a double gap, a zero-bias conductance peak, and a broad conductance overshoot at the gap edge. These anomalies are not reproducible. On the other hand, spectra containing a small zero-bias conductance of less than 20% of $G_{\text{obs}}(V=100 \text{ mV}, T)$ typically show a reliable single-gap feature with a sharp overshoot at the gap edge. Representative data for this group are summarized in Fig. 2. The zero-bias conductances of samples A, B, and C are 16%, 10%, and 13%, respectively. Since all junctions in Fig. 2 show the distinct V-shaped backgrounds, it is difficult to determine the precise quasiparticle DOS. To determine the real DOS, the measured tunneling spectra should be systematically

deconvoluted into two components, namely, a normal-state background and a quasiparticle DOS at all temperatures. This deconvolution has been performed in three steps. First, we have determined a fitting function for the background conductance $G_V(V, T)$ above T_c . Second, the background conductance below the T_c is inferred by extrapolation using this function. Finally, the measured

tunneling spectra $G_{\text{obs}}(V, T)$ is compared with a calculated curve $G_{\text{cal}}(V, T)$ based on a theory for the effective DOS convoluting the superconducting gap with the voltage- and temperature-dependent background.

The calculated tunneling conductance G_{cal} across a normal-metal-insulator-superconductor (N - I - S) junction is given by

$$G_{\text{cal}}(V, T) = \int_{-\infty}^{\infty} |M|^2 N_1(E) N_2(E) [-df(E - eV)/d(eV)] dE, \quad (1)$$

where $N_1(E)$ is the effective DOS of the superconductor, $N_2(E)$ is the DOS of the normal metal, M is the tunneling matrix element, and f is the Fermi function, $f = [1 + \exp(eV/k_B T)]^{-1}$.³⁴ Equation (1) can be simplified by assuming that M is independent of the voltage and $N_2(E)$ is constant near the Fermi level. Since the tunneling conductance of high- T_c superconductors shows a temperature-dependent background curve, it is convenient to normalize the tunneling conductance at $V=100$ mV for comparison between the experimental and theoretical conductance curves. The normalized theoretical conductance can be written

$$G_{\text{cal}}(V, T) = A |M|^2 N_2 \times \int_{-\infty}^{\infty} N_e(E) [-df(E - eV)/d(eV)] dE, \quad (2)$$

where A is a coefficient and $N_e(E)$ is the effective DOS, which is a distribution function convoluting the superconducting gap with the background curve. The integral of $N_e(E)$ is normalized to unity at $V=100$ mV. $A |M|^2 N_2$ corresponds to $G_{\text{obs}}(V=100 \text{ mV}, T)$.

The normalized conductance curves $G_{\text{obs}}(V, T)/G_{\text{obs}}(V=100 \text{ mV}, T)$ for the junctions A, B, and C just above T_c are presented in Fig. 3. The curves show a linear voltage dependence above 30 mV and a round bottom at zero bias. In every junction, the ob-

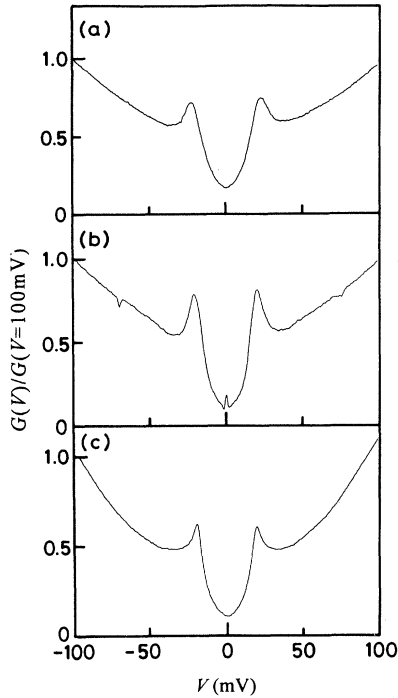


FIG. 2. Tunneling conductance $G(V, T=11 \text{ K})$ of three Au/Bi₂Sr₂CuO₆/Bi₂Sr₂CaCu₂O₈ junctions: (a) junction A, (b) junction B, and (c) junction C. The spectra are normalized to unity at $V=100$ mV, and for each junction, the zero-bias conductances are lower than 20% of $G_{\text{obs}}(V=100 \text{ mV}, T=11 \text{ K})$. All spectra show a symmetric and single-gap feature with sharp overshoots at the gap edges superimposed on a V-shaped background.

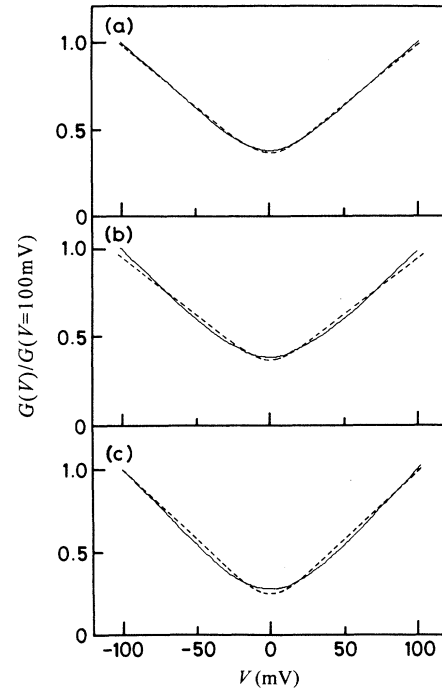


FIG. 3. $G(V, T=90 \text{ K})$ fits to data at just above T_c : (a) sample A, (b) sample B, and (c) sample C. Solid curves are the observed conductances $G_{\text{obs}}(V, T=90 \text{ K})$ normalized to unity at $V=100$ mV. The dashed curves $G_V(V, T=90 \text{ K})$ were calculated from Eq. (3) using the linear background function of Eq. (4) for samples A, B, and C, respectively.

served conductance curves $G_{\text{obs}}(V, T)$ can be fitted with a V-shaped background curve $G_V(V, T)$ calculated from Eq. (2) using a V-shaped background function N_V :

$$G_V(V, T) = G_{\text{obs}}(V=100 \text{ mV}, T) \times \int_{-\infty}^{\infty} N_V(E, T) [-df(E - eV)/d(eV)] dE, \quad (3)$$

where

$$N_V(E, T) = N_0(T) + m(T)|E|. \quad (4)$$

$N_0(T)$ is the zero-bias value, and $m(T)$ is the slope of the linear voltage dependence. Since the $N_V(E, T)$ is normalized to unity at $V=100 \text{ mV}$, the slope m can be expressed as a function of N_0 according to

$$m(T) = 10[1 - N_0(T)]. \quad (5)$$

Therefore the slope and zero-bias conductance of $G_V(V, T)$ are uniquely determined by only one parameter $N_0(T)$. Furthermore, the curvature around zero bias can be well fitted by thermal broadening of the kink in the function $N_V(E, T)$ at zero bias without additional parameters.

Figure 4 shows the temperature dependence of observed conductance curves $G_{\text{obs}}(V, T)$ (solid line) above T_c in each case normalized to unity at $V=100 \text{ mV}$. With decreasing temperature, the slope increases and the curvature around zero bias becomes sharper. The fitting curve $G_V(V, T)$ (dashed line) obtained from Eq. (3) agrees with $G_{\text{obs}}(V, T)$ over the entire temperature interval 300

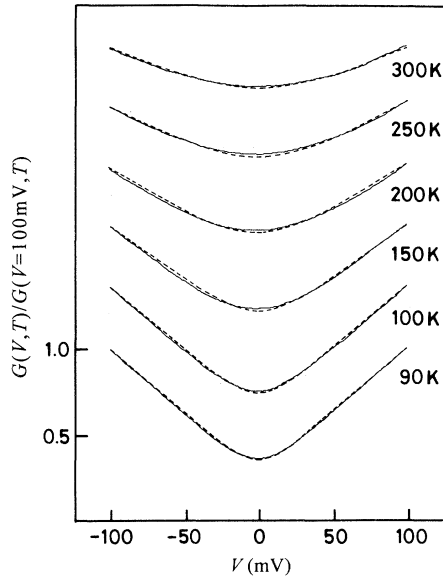


FIG. 4. Fits to the $G_{\text{obs}}(V, T)$ data for junction A in the range 90–300 K. The solid curves are the observed conductances $G_{\text{obs}}(V, T)$ normalized to unity at $V=100 \text{ mV}$. The scale of the normalized conductance applies to the $T=90 \text{ K}$ curve; the other curves have been shifted for clarity. The dashed curves $G_V(V, T)$ were calculated from Eq. (3) using the linear background function of Eq. (4) at each temperature.

$K > T > T_c$ via the choice of only one fitting parameter $N_0(T)$. This result indicates that the temperature dependence of $G_{\text{obs}}(V, T)$ and the curvature around zero bias can be well understood by the V-shaped background function $N_V(E, T)$, thermally broadened by the Fermi function. The values of $N_0(T)$ and $m(T)$ reflect the zero-bias conductance and the slope of the normalized linear background, respectively. On the other hand, the actual $G_V(V, T)$ curve including the conductance amplitude is given by the values of $G_{\text{obs}}(V=100 \text{ mV}, T)N_0(T)$ and $G_{\text{obs}}(V=100 \text{ mV}, T)m(T)$. Figure 5(a) shows the plots of $\ln[G_{\text{obs}}(V=100 \text{ mV}, T)N_0(T)]$ and $\ln[G_{\text{obs}}(V=100 \text{ mV}, T)m(T)]$ as a function of temperature for sample A. We have found the empirical relation that $\ln[G_{\text{obs}}(V=100 \text{ mV}, T)N_0(T)]$ and $\ln[G_{\text{obs}}(V=100 \text{ mV}, T)m(T)]$ obtained from fits using Eq. (3) both show a linear dependence on the temperature. These linear dependences indicate that the actual zero-bias conductance $G_{\text{obs}}(V=100 \text{ mV}, T)N_0(T)$ increases exponentially with T according to the relation $G_{\text{obs}}(V=100 \text{ mV}, T)N_0(T) = \exp(0.68 + 6.1 \times 10^{-3} T)$. On the other hand, the actual slope $G_{\text{obs}}(V=100 \text{ mV}, T)m(T)$ decreases exponentially with increasing T as $G_{\text{obs}}(V=100$

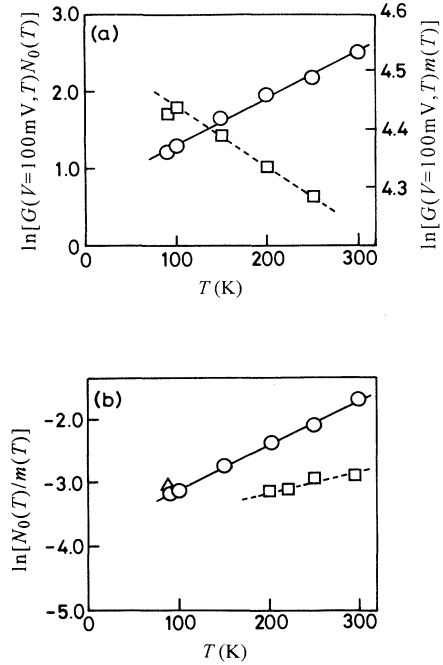


FIG. 5. (a) Temperature dependence of $G_{\text{obs}}(V=100 \text{ mV}, T)N_0(T)$ (open circles) and $G_{\text{obs}}(V=100 \text{ mV}, T)m(T)$ (open squares) obtained from the fits for sample A shown in Fig. 4, using the background function of Eq. (4). The solid line is $G_{\text{obs}}(V=100 \text{ mV}, T)N_0(T) = \exp(0.68 + 6.1 \times 10^{-3} T)$ and the dashed line is $G_{\text{obs}}(V=100 \text{ mV}, T)m(T) = \exp(4.5 - 1.1 \times 10^{-3} T)$. The parameters a, b were determined by a least-mean-squares method. (b) Temperature dependence of $N_0(T)/m(T)$ as derived from fits using the background function of Eq. (4): open circles, open triangles, and open squares for junctions A, B, and C, respectively. The solid line is $N_0(T)/m(T) = \exp(-3.8 + 7.2 \times 10^{-3} T)$ for junction C.

$mV, T)m(T) = \exp(4.5 - 1.1 \times 10^{-3}T)$. These empirical relations are satisfied in the temperature range from T_c to 300 K. However, these plots cannot be used directly for extrapolation to below T_c because $G_{\text{obs}}(V=100 \text{ mV}, T)$ may be affected by the tail of the superconducting gap structure. This problem may be circumvented by using the ratio of $G_{\text{obs}}(V=100 \text{ mV}, T)N_0(T)$ to $G_{\text{obs}}(V=100 \text{ mV}, T)m(T)$ in the extrapolation. In this ratio, the $G_{\text{obs}}(V=100 \text{ mV}, T)$ term is canceled out, while a new exponential relation is obtained. A plot of $\ln[N_0(T)/m(T)]$ as a function of T is shown in Fig. 5(b). This plot also indicates a linear dependence on temperature which can be used for extrapolation below T_c . This linear relation is

$$\begin{aligned} \ln[N_0(T)/m(T)] &= \ln\{N_0(T)/[10(1-N_0(T))]\} \\ &= a + bT, \end{aligned} \quad (6)$$

where $a = -3.8$ and $b = 7.2 \times 10^{-3}$ for junction A (solid line) and $a = -3.8$ and $b = 8.7 \times 10^{-3}$ for junction C (dashed line). A similar relation could not be derived for junction B because no data were obtained above T_c . However, since the spectrum of junction B at 90 K agrees well with that of junction A, we assume that the line for junction A is also applicable for junction B. From Eq. (6), $N_0(T)$ can be solved as

$$N_0(T) = 10 \exp(a + bT) / [1 + 10 \exp(a + bT)]. \quad (7)$$

Figure 6 shows $N_0(T)$ for junction A (solid line) and C (dashed line) calculated from Eq. (7). The predicted background curve below T_c is determined by the N_0 value obtained from this relation. We will discuss below whether or not this extrapolation is physically plausible.

In Fig. 7, the solid line indicates the observed conductance curve $G_{\text{obs}}(V, T)$ below T_c and the dashed line indicates the V-shaped background curves $G_V(V, T)$ calculated from Eq. (3) using the N_0 value extrapolated from Eq. (7). These curves are normalized to unity at $V=100 \text{ mV}$.

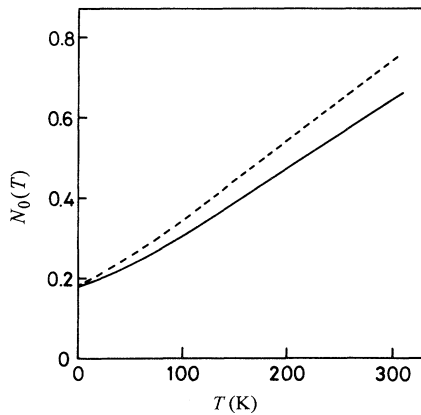


FIG. 6. Temperature dependence of $N_0(T)$ calculated from Eq. (7) with the parameters $a = -3.8$, $b = 7.2 \times 10^{-3}$ for junction A (solid line) and $a = -3.8$, $b = 8.7 \times 10^{-3}$, $b = 3.8$ for junction C (dashed line), as obtained from the fits using Eq. (6) and shown in Fig. 5(b).

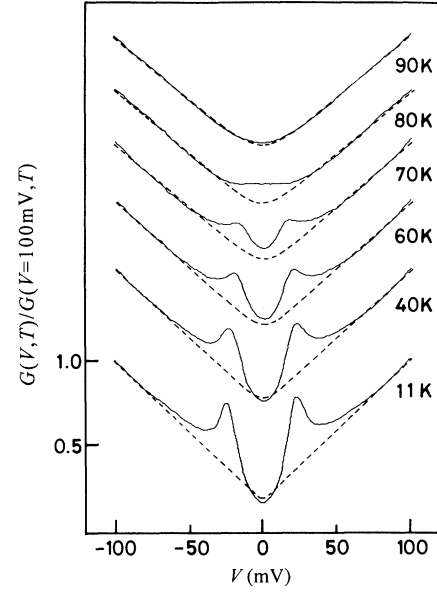


FIG. 7. Temperature-dependent tunneling conductance $G_{\text{obs}}(V, T)$ below T_c for sample A (solid line) and predicted background conductance $G_V(V, T)$ (dashed line) as obtained by the extrapolation shown in Fig. 6, using Eq. (7). The scale of the normalized conductance applies to the $T=11 \text{ K}$ curve; the other curves have been shifted for clarity. With decreasing temperature, the predicted V-shaped background becomes deeper and the kink at zero bias becomes sharper. The observed zero-bias conductance $G_{\text{obs}}(V=0 \text{ mV}, T)$ is equal to or larger than the extrapolated $G_V(V=0 \text{ mV}, T)$ for all temperatures.

It is seen that the $G_V(V, T)$ curve fits the $G_{\text{obs}}(V, T)$ curves well for all temperatures in the voltage region outside gap. This result suggests that this extrapolation may be interpreted as the normal-state conductance at large bias voltage. However, this interpretation leads to the difficulty that simple BCS theory and the lifetime smearing model of Dynes cannot be directly applied to the fitting of the observed gap structure. This is because the observed conductance around zero bias is larger than the predicted normal-state conductance. Consequently, the conservation of the DOS outside and inside the gap edge is not maintained as a result of the excess current observed in the gap region. Figure 8 shows a plot of the normalized zero-bias conductance $G_{\text{obs}}(V=0 \text{ mV}, T)/G_{\text{obs}}(V=100 \text{ mV}, T)$ as a function of T . The solid line indicates the temperature dependence of the normalized zero-bias conductance $G_V(V=0 \text{ mV}, T)/G_V(V=100 \text{ mV}, T)$ for the predicted V-shaped background. Since the excess currents appear just below T_c , it appears that this excess current is related to the superconductivity. This anomaly can be interpreted by Andreev reflection³⁵ induced by the semiconductive $\text{Bi}_2\text{Sr}_2\text{CuO}_6$ layer. In the case of N - S junctions, the outward superconducting DOS including Andreev reflection can be written in a simple form

$$\begin{aligned} N_{\text{Andreev}}(E, \Delta, Z) \\ = 2(1 + Z^2)[1 + A(E, \Delta, Z) - B(E, \Delta, Z)], \end{aligned} \quad (8)$$

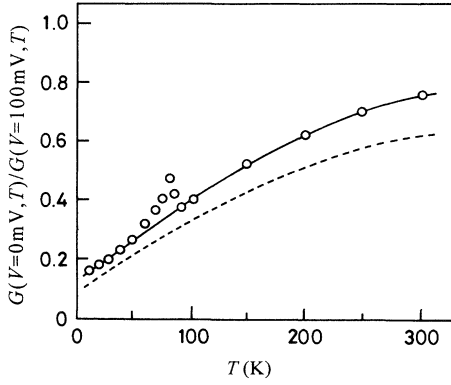


FIG. 8. Temperature dependence of the normalized zero-bias conductance $G_{\text{obs}}(V=0 \text{ mV}, T)/G_{\text{obs}}(V=100 \text{ mV}, T)$ for junction A showing a remarkable discontinuity at T_c . The solid curve was obtained from Eq. (3) using the parameters derived from the fits to the background conductance above T_c for junction A. The dashed curve was derived from marginal-Fermi-liquid theory (Ref. 47).

where $A(E, \Delta, Z)$ is the probability of Andreev reflection and $B(E, \Delta, Z)$ is the probability of normal reflection.³⁶ $A(E, \Delta, Z)$ and $B(E, \Delta, Z)$ have the following functional forms:

$$A(E, \Delta, Z) = \Delta^2 / [E^2 + (\Delta^2 - E^2)(1 + Z^2)^2],$$

$$B(E, \Delta, Z) = 1 - A(E, \Delta, Z) \text{ for } E < \Delta$$

and

$$A(E, \Delta, Z) = u_0^2 v_0^2 / \gamma^2,$$

$$B(E, \Delta, Z) = [(u_0^2 - v_0^2)^2 Z^2 (1 + Z^2)] / \gamma^2 \text{ for } E > \Delta,$$

with

$$\gamma^2 = [u_0^2 + Z^2(u_0^2 - v_0^2)]^2$$

and

$$u_0^2 = 1 - v_0^2 = \frac{1}{2} \{ 1 + [(E^2 - \Delta^2)/E^2]^{1/2} \},$$

where Δ is the gap energy. For convenience, a dimensionless barrier strength $Z = H/hv_F$ has been introduced in Eq. (8), where H is the barrier height and v_F the Fermi velocity. The elegance of this expression is that junctions with different barrier transparencies can be treated in a similar fashion by the barrier strength expressed through this dimensionless parameter Z . In the case of $Z=0$, which corresponds to a clean N - S interface, the conductance inside the gap is calculated a factor of 2 higher than in the normal state. On the other hand, in the case of a

high barrier ($Z > 10$), N_{Andreev} agrees with the simple BCS density-of-states function.

For fitting to the data, we have tested three procedures for the convolution of the gap structure and background for junction A at $T=11 \text{ K}$. These procedures reflect different origins for the V-shaped background. The actual background curve is obtained from the extrapolation shown in Fig. 7, using Eq. (7), which gives $N_0=0.188$ at $T=11 \text{ K}$. In the first model, it is assumed that the linear background is not related to electron tunneling from the superconductor. The total conductance then is given by the sum of the linear background and the superconducting gap structure. These two components are regarded as independent processes without any relation to each other. Assuming that the predicted linear background includes the normal-state conductance $N_n(T)$, which is independent of the bias voltage, the effective DOS $N_e(E)$ can be written as

$$N_e(E, T) = N_V(E, T) - N_n(T) + N_n(T)N_s(E), \quad (9)$$

where $N_s(E)$ is the superconducting DOS normalized to unity at $|E| = \infty$. The components of the linear voltage dependence and the superconducting gap structure correspond to $N_V(E, T) - N_n(T)$ and $N_n(T)N_s(E)$, respectively. The contribution of each component to the total conductance is determined by the value of $N_n(0)$. This value lies in the range $0 < N_n(T) \leq N_0(T)$. Figure 9(a) shows $G_{\text{cal}}(V, T=11 \text{ K})$ calculated from Eq. (2) using the effective DOS $N_e(E)$ given by Eq. (9), which is compared to the $G_{\text{obs}}(V, T=11 \text{ K})$ data for junction A. The dot-dashed curve represents the inferred linear background corresponding to the component $N_V(E, T) - N_n(T)$. Setting $N_s(E)=1$ gives $G_{\text{cal}}(V, T) = G_V(V, T)$, which indicates the normal-state conductance curve including the linear background (dotted line). The dashed curve indicates the total conductance calculated using the BCS DOS with Andreev reflection, where $N_s(E) = N_{\text{Andreev}}(E, \Delta=22.5 \text{ meV}, Z=0.53)$ and $N_n = N_0 = 0.188$. The zero-bias conductance and curvature around zero bias of $G_{\text{obs}}(V, T)$ can be fitted through a choice of the parameters Δ and Z . However, the conductance peaks of $G_{\text{cal}}(V, T)$ at the gap edge are smaller than those of $G_{\text{obs}}(V, T)$ despite using the maximum value of the normal-state DOS $N_n(0) = N_0$. Consequently, this model does not provide a good fit of the observed data $G_{\text{obs}}(V, T)$.

Second, we have tested a fitting model based on inelastic scattering. In this model, the contribution of the linear background to total conductance vanishes inside the gap because the scattering process involves quasiparticle electron tunneling from the superconductor.³⁷ Therefore the effective DOS $N_e(E, T)$ is given by

$$N_e(E, T) = \begin{cases} N_V(E, T) - N_V(\Delta, T) + N_V(\Delta, T)N_s(E) & \text{for } E > |\Delta|, \\ N_V(\Delta, T)N_s(E) & \text{for } E < |\Delta|. \end{cases} \quad (10)$$

The observed data $G_{\text{obs}}(V, T)$ of junction A and the calculated conductance $G_{\text{cal}}(V, T)$ are compared in Fig. 9(b). The dot-dashed curve indicates the inelastic conductance, corresponding to the component $N_V(E, T) - N_V(\Delta, T)$ in Eq. (10). The dotted curve represents the normal-state conductance including the linear background $G_{\text{cal}}(V, T) = G_V(V, T)$, obtained by setting $N_s(E) = 1$. The

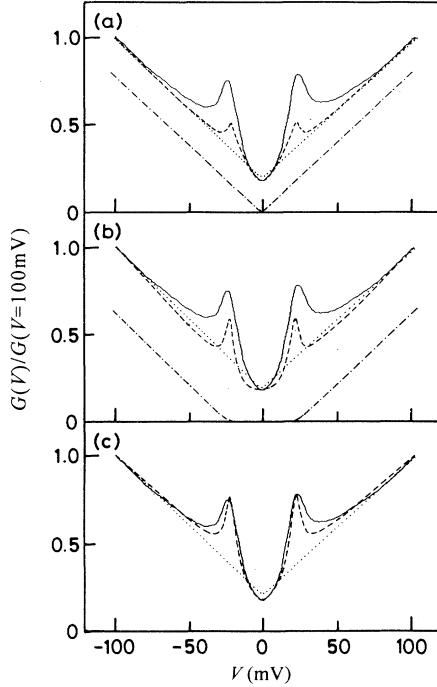


FIG. 9. (a) Fits to the $G_{\text{obs}}(V, T)$ data for junction A at 11 K using Eq. (9), assuming that the total conductance is obtained by the sum of the linear background and the superconducting DOS. The solid curve is the observed data $G_{\text{obs}}(V, T=11 \text{ K})$. The dashed line is total conductance calculated from the BCS function including Andreev reflection, where $N_s(E) = N_{\text{Andreev}}(E, \Delta = 22.5 \text{ meV}, Z = 0.53)$ and $N_n(T) = N_0(T = 11 \text{ K}) = 0.188$. The dotted curve is the normal-state conductance including the linear background, as shown in Fig. 7, when $N_s(E) = 1$. The dot-dashed curve represents the linear background component. (b) Fits to the $G_{\text{obs}}(V, T)$ data for junction A at 11 K using Eq. (10), assuming the inelastic scattering model. The solid curve is the observed data $G_{\text{obs}}(V, T = 11 \text{ K})$. The dashed curve is the inelastic tunneling conductance calculated from the BCS function including Andreev reflection, where $N_s(E) = N_{\text{Andreev}}(E, \Delta = 22.5 \text{ meV}, Z = 0.8)$ and $N_0(T = 11 \text{ K}) = 0.188$. The dotted curve is the normal-state conductance including inelastic scattering, as shown in Fig. 7, when $N_s(E) = 1$. The dot-dashed curve represents the component of the inferred inelastic scattering. (c) Fits to the $G_{\text{obs}}(V, T)$ data for junction A at 11 K using Eq. (11), assuming a density-of-states effect. The solid curve is the observed data $G_{\text{obs}}(V, T = 11 \text{ K})$. The dashed curve is total conductance calculated from the BCS function including Andreev reflection, where $N_s(E) = N_{\text{Andreev}}(E, \Delta = 22.5 \text{ meV}, Z = 0.64)$ and $N_0(T = 11 \text{ K}) = 0.188$. The dotted curve is the normal-state conductance when $N_s(E) = 1$.

dashed curve indicates the total conductance calculated by using the BCS function with Andreev reflection, where $N_s(E) = N_{\text{Andreev}}(E, \Delta = 22.5 \text{ meV}, Z = 0.80)$ and $N_n = N_0 = 0.188$. The fit has been evaluated at the zero-bias conductance and the peak-top position of the gap edge. The zero-bias conductance agrees well with the observed data $G_{\text{obs}}(V, T)$ through the choice of the barrier strength Z . However, the curvature of the bottom of the gap and the conductance peak at the gap edge cannot be fitted to $G_{\text{obs}}(V, T)$. Therefore this model also does not provide an adequate description of the observed data.

Finally, we have tested a model in which the linear background reflects the DOS of the bulk of the superconducting material. In this model, the total conductance is given as the product of the normal-state DOS and the superconducting DOS. The total conductance is often calculated by using the relation $G(V, T) = G_V(V, T)G_s(V, T)$, where $G_s(V, T)$ is the conductance calculated from $N_s(E)$ convoluted with $-df/d(eV)$. However this gives correct conductance values only for $T \ll T_c$. To discuss the temperature dependence of the gap structure, the total conductance should be calculated using the integral of Eq. (2) and the effective DOS given by

$$N_e(E, T) = N_V(E, T)N_s(E). \quad (11)$$

Figure 9(c) compares the calculated conductance $G_{\text{cal}}(V, T)$ with the observed data $G_{\text{obs}}(V, T)$ at $T = 11 \text{ K}$. Setting $N_s(E) = 1$ yields the normal-state conductance (dotted line). The dashed curve represents the total conductance calculated from the BCS gap function including the Andreev reflection, $N_s(E) = N_{\text{Andreev}}(E, \Delta = 22.5 \text{ meV}, Z = 0.64)$, which reproduces completely the zero-bias conductance and curvature inside the gap. This result indicates that this model may be suitable for the fitting.

Using this fitting procedure, we have extended the calculation of the gap structure to higher temperatures below T_c . The observed gap structure $G_{\text{obs}}(V, T)$ can be fitted by $G_{\text{cal}}(V, T)$ calculated from $N_{\text{Andreev}}(E, \Delta, Z)$ at low temperatures. However, at higher temperatures, the $G_{\text{obs}}(V, T)$ curve is broader than that of $G_{\text{cal}}(V, T)$. The quasiparticle relaxation time near T_c becomes so short that the lifetime broadening cannot be neglected. Accordingly, the temperature-dependent fitting curves were calculated by the outward DOS including lifetime smearing³⁸ given by

$$N_{\text{Andreev}}^{\text{LT}}(E, \Delta, Z, \Gamma) = \text{Re}[N_{\text{Andreev}}(E + i\Gamma, \Delta, Z)]. \quad (12)$$

Figure 10 shows the $G_{\text{obs}}(V, T)$ of sample A and $G_{\text{cal}}(V, T)$ below T_c calculated from Eq. (12). The zero-bias conductance and the curvature around zero bias can be reproduced completely by choosing the fitting parameters $\Delta(T)$, $\Gamma(T)$, and $Z(T)$. However, the conductance peaks of $G_{\text{cal}}(V, T)$ at the gap edge are smaller than those of $G_{\text{obs}}(V, T)$ for all temperatures.

At low temperature, the gap values $2\Delta = 45, 43,$ and 41 meV were obtained from these fits for functions A, B, and C, respectively. These values correspond to a ratio of $2\Delta/kT = 5.2 - 6.0$ which is larger than that for conven-

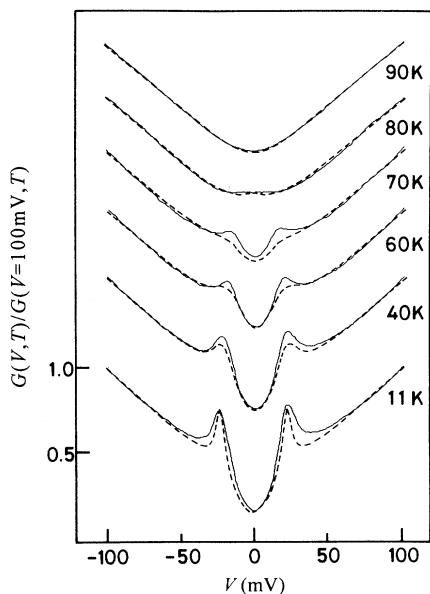


FIG. 10. Fits to the $G_{\text{obs}}(V, T)$ data of junction A below T_c . The solid curves are observed conductances $G_{\text{obs}}(V, T)$ normalized to unity at $V=100$ mV. The scale of the normalized conductance applies to the $T=11$ K curve; the other curves have been shifted for clarity. The dashed curves are $G_{\text{cal}}(V, T)$ calculated from Eq. (11), where $N_s(E) = N_{\text{Andreev}}^{LT}(E, \Delta, Z, \Gamma)$ at each temperature. The shape of the gap structure around zero bias is well reproduced by the calculation. However, the calculated conductance peak at the gap edge is lower than that of observed data.

tional BCS superconductors. However, in Fig. 11, it is seen that the temperature dependence of $\Delta(T)$ for junction A agrees well with the BCS curve (solid line) scaled to bulk $T_c=84$ K. Figure 12 shows the temperature dependence of the fitted value of $\Gamma(T)$ for junction A. The $G_{\text{obs}}(V, T)$ data for $T < 40$ K can be fitted accurately without lifetime smearing because the lifetime broadening is much smaller than the thermal broadening. Ac-

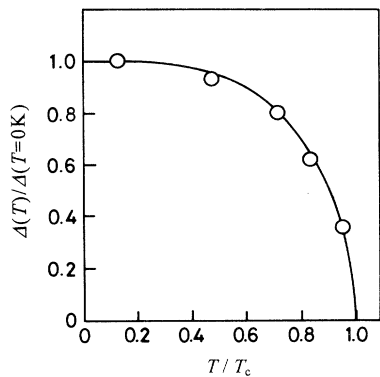


FIG. 11. Temperature dependence of the gap energy $\Delta(T)$ from the fits in Fig. 10 for junction A. The solid curve represents BCS theory scaled to $T=84$ K, which is the T_c of the bulk $\text{Bi}_2\text{Sr}_2\text{CaCu}_2\text{O}_8$ single crystal.

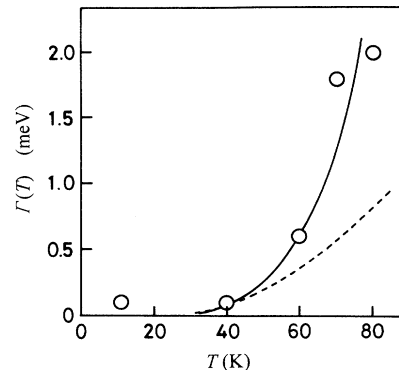


FIG. 12. Temperature dependence of the lifetime broadening $\Gamma(T)$ derived from the fits in Fig. 10 for junction A. The data at 11 and 40 K represent upper limits for the Γ value. The solid line is a guide to the eye. The dashed curve indicates a $(T/T_c)^3$ dependence.

cordingly, the exact values of Γ below 40 K cannot be determined from the conductance curves and the 11- and 40-K data included in Fig. 12 are estimated upper limit values of Γ . The $\Gamma(T)$ value increases dramatically upon approaching T_c . For comparison to our data, the $(T/T_c)^3$ dependence is represented by dashed line and discussed below.

IV. DISCUSSION

A. Linear background

We found that the background conductance in the tunneling spectra along the c axis can be described by a linear function including thermal smearing. A linear background has been reported for different kinds of junctions, especially for c -axis tunneling.⁷⁻¹³ The origin of this background has been attributed to several mechanisms, such as a charging effect, voltage-dependent tunneling penetration probabilities, a density-of-states effect, and inelastic scattering. The first of these possibilities, the charging effect, predicts linear backgrounds for a distribution of effective capacitors in the tunneling region.^{39,40} However, this effect could occur in junctions in which it appears unlikely that isolated metallic regions are included in the epitaxial barrier region. Furthermore, in this model, the observed conductance overshoots do not necessarily arise at the superconducting gap edge, contrary to what has been observed in the present investigation. A second mechanism involves voltage-dependent tunneling penetration probabilities.⁴¹ However, it is difficult to reproduce the sharpness of the experimentally observed discontinuities in the slope of the conductance curves at zero-bias voltage using this model. A third possible mechanism would involve inelastic tunneling.^{37,42-44} In this case, it has been proposed that the superconductive DOS may be derived by simple subtraction of the inferred inelastic conductance from the total conductance.³⁷ However, as already examined in this paper

[see Fig. 9(b)], this deconvolution process is not suitable. The fourth mechanism evokes a density-of-states effect.^{45–48} The observed conductance curve is well fitted by the product of the BCS function including Andreev reflection and the extrapolated linear background as shown in Fig. 9(c). This result suggests that this linear background reflects the normal-state DOS in the bulk of the high- T_c superconducting material.

This DOS effect was interpreted in terms of resonating-valence-band (RVB) model.⁴⁵ In this picture, the tunneling carriers excite both charge and spin degrees of freedom in the high- T_c superconductor. A conductance which varies linearly with the voltage can be understood by integration over one of these degrees of freedom. In gauge-field theory, however, it is pointed out that the linear bias dependence would occur only for added holes,⁴⁹ which is in disagreement with the observation of linear conductances for both positive and negative bias as shown in Fig. 2. Furthermore, the RVB model predicts a deviation of the superconducting DOS from BCS theory.⁴⁵ However, our results suggest that the superconducting DOS is well fitted by BCS theory, which has been the basis for the fits in Figs. 9(c) and 10. Alternatively, a DOS effect on the linear conductance may be attributed to anisotropic metal characteristics using marginal-Fermi-liquid (MFL) phenomenology, which also leads to a linear background conductance for c -axis tunneling.⁴⁷ In this model, there is no modification of the superconducting DOS from the BCS predictions in accordance with the fit in Fig. 9(c). Moreover, as shown in Fig. 8, the temperature dependence of the conductance ratio $G_{\text{obs}}(V=0 \text{ mV}, T)/G_{\text{obs}}(V=100 \text{ mV}, T)$ (solid curve) is qualitatively similar to the theoretical result in the MFL model (dashed curve).⁴⁷ Accordingly, the MFL model appears to provide an adequate description of the linear conductance. The MFL model leads to an s -wave pairing state, which is consistent with the s -wave-like character of the superconducting gap structure, as discussed below.

The temperature dependence of the V-shaped background above T_c can be described by a simple empirical expression as given in Eq. (4). The question of whether this temperature dependence can be extrapolated to temperatures below T_c is important for the deconvolution of the $G_{\text{obs}}(V, T)$ data to derive the intrinsic superconducting DOS. Our results indicate that the V-shaped background function $N_V(N_0, E)$ can indeed be extrapolated to lower temperatures, as shown by the fits of Fig. 9(c). By contrast, a conductance minimum at $V=0$, which only occurs at temperatures just above T_c , has been reported for planar junctions along c axis using a native barrier.²⁷ This conductance minimum has been interpreted in terms of localization along the c axis. In our data, however, the gap feature opens up just at T_c and does not indicate a localization effect.

B. Andreev reflection

The data always show an excess current in the gap region as shown in Fig. 7. In the fitting procedure, we have assumed that this excess current is caused by Andreev

reflection, because the conductance varies in the same way as the conductance overshoot at the gap edge. Furthermore, the conductance maximum is less than 2 times the inferred normal-state conductance and the excess current vanishes precisely at T_c in the temperature-dependent spectra. This behavior is similar to that recently reported for Ag-YBa₂Cu₃O_{7- δ} .⁵⁰ The assumed role of Andreev reflection is further supported by the fact that the observed excess current exhibits a quite different behavior than the zero-bias conductance peak (ZBCP). The observed conductance maximum has a broader structure than that of the ZBCP induced by quasiparticle tunneling, phase diffusion, or supercurrent.^{10,15,25,51} On the other hand, the ZBCP induced by Appelbaum-Kondo model for electron magnetic interaction shows a broad peak centered at $V=0$ similar to Andreev reflections.^{52,53} However, this case can be easily distinguished from Andreev reflection, because the excess current induced by the Appelbaum-Kondo effect persists above T_c .

In the Au/Bi₂Sr₂CuO₆/Bi₂Sr₂CaCu₂O₈ system, the Bi₂Sr₂CuO₆ layer is a semiconductor and the barrier height of this junction is lower than those of conventional planar junctions using barrier materials such as MgO or CaF₂. Accordingly, the semiconductive layer of Bi₂Sr₂CuO₆ may be responsible for the excess current generated by Andreev reflection. If electron tunneling occurs from the Au layer to the Bi₂Sr₂CaCu₂O₈ single crystal, the Bi₂Sr₂CuO₆ layer plays the role of a low barrier as shown in Fig. 13(a). This idea seems to be unreal-

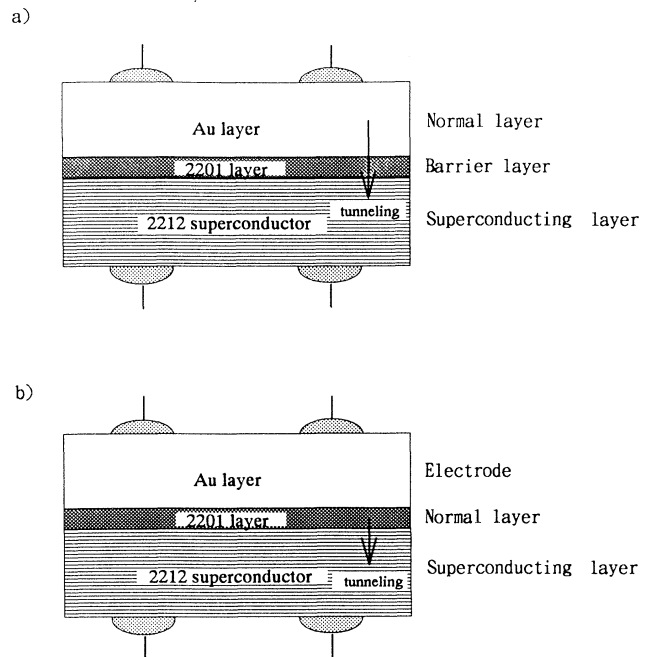


FIG. 13. Schematic of two possible tunneling geometries for the Au/Bi₂Sr₂CuO₆/Bi₂Sr₂CaCu₂O₈ junction. (a) Model assuming that the electron tunneling occurs from the AU layer to the Bi₂Sr₂CaCu₂O₈ single crystal via the 2201 barrier layer. (b) Model assuming that the electron tunneling occurs from the Bi₂Sr₂CuO₆ layer to the Bi₂Sr₂CaCu₂O₈ single crystal.

istic because the junction resistance of $10^3 \Omega \text{ cm}$ is much larger than that in N - S point-contact experiments on conventional superconductors.^{54,55} However, since Andreev reflection has often been reported for S - I - N junctions using high- T_c superconductors,^{56–58} this model cannot be entirely ruled out. A second idea is that the electron tunneling occurs between the $\text{Bi}_2\text{Sr}_2\text{CuO}_6$ layer and the $\text{Bi}_2\text{Sr}_2\text{CaCu}_2\text{O}_8$ single crystal. In this case, the barrier exists at the interface between these layers and the role of the $\text{Bi}_2\text{Sr}_2\text{CuO}_6$ layer is that of a normal metal in N - S junctions as shown in Fig. 13(b). To identify the real barrier, further experiments on junctions using various thicknesses of $\text{Bi}_2\text{Sr}_2\text{CuO}_6$ layers will be required.

It has often been reported in the literature that there is a violation of conservation of the DOS inside and outside the gap in the tunneling conductance data for HTSC's. We suspect that this anomaly can be attributed to the role of Andreev reflections because, in many cases, a degraded layer of the superconductor may be present at the interface of the tunnel junction, which could play the role of a normal-metal layer in low barrier N - S junctions. On the other hand, it has been pointed out that the tunneling spectra obtained by STM can also be interpreted in the framework of Andreev reflections.⁵⁹ Since the barrier thickness in this case is much smaller than that of traditional planar junctions, STM junctions may be regarded as N - S junctions. In fact, the action of STM is based on the existence of an excess current which changes with the distance between the tip and surface of the superconductor.²¹ Our experiments provide typical and systematic data in the presence of low barrier heights as mentioned above.

C. $\Delta(T)$ and $\Gamma(T)$

At low temperature, gap values of $2\Delta = 43\text{--}45 \text{ meV}$ are obtained from the fits to the present experiments. These values correspond to $2\Delta/kT = 5.4\text{--}6.0$, which is smaller than most of the previously reported data, $2\Delta/k_B T_c \sim 8$. In many cases, previous tunneling measurements have yielded the maximum value of the anisotropic order parameter because of mixing of the tunneling current along both the c axis and ab plane as a result of an imperfect interface. The value of $2\Delta/k_B T_c = 5.7$ obtained in this work for an epitaxial tunneling junction may reflect the c -axis component of the anisotropic order parameter. In fact, this value is consistent with reported estimates for the gap anisotropy along ab and c , which are in the range $1.5\text{--}1.8$.^{16,60,61}

Figure 10 shows the temperature dependence of the tunneling conductance. With increasing temperature, the gap structure becomes narrower and finally disappears at $T = 85 \text{ K}$. The temperature dependence of $\Delta(T)$ agrees well with the BCS curve as shown in Fig. 11. The zero gap temperature T_c (tunneling) estimated from the BCS curve is $85 \pm 2 \text{ K}$, which is equal to $T_c = 84 \text{ K}$ derived from the resistivity measurements. This agreement suggests that virtually no degradation of the superconductivity has taken place at the junction interface and that the measurements should reflect the true DOS. This

behavior is quite different from that in reports where $\Delta(T)$ remains finite at T_c owing to fluctuations.^{26,27}

In our earlier paper we reported a sharp gap structure for the epitaxial tunneling junction and a small broadening $\Gamma = 2 \text{ meV}$ at 10 K obtained with the lifetime smearing model.³² This value is substantially smaller than that reported previously with values for Γ in the range of $10\text{--}20 \text{ meV}$.^{10,17,18,26,27} We suspect that such large broadening is not intrinsic for the superconductivity mechanism, but should be attributed to imperfections of the interface. In the present experiments and analysis, we found that the lifetime broadening is even smaller than that of our earlier report as shown in Fig. 12. Below 40 K , the lifetime broadening can be neglected because it is much smaller than thermal broadening. At these temperatures, the value of Γ cannot be determined accurately from the fits. Only an upper limit of $\Gamma \sim 0.1 \text{ meV}$ can be estimated. This implies that the quasiparticle recombination time exceeds 10 ps , which is about 10 times larger than times estimated from high-energy excitation measurements of the transient reflectivity using a femtosecond pulsed laser.⁶² If we assume that the recombination is due to electron-phonon coupling, then it follows that the 2212 superconductor has a very strong electron-phonon coupling. The quasiparticle lifetime is the same or one order of magnitude shorter than that of the electron-phonon coupling in the alloy $\text{Pb}_{0.9}\text{Bi}_{0.1}$.³⁸

As the temperature approaches T_c , the lifetime broadening increases dramatically as shown in Fig. 12. $\Gamma(T)$ rises more rapidly than the T^3 dependence of the pair-breaking rate (indicated by the dotted line), suggested as being intrinsic for the in-plane cuprate superconductors.^{26,63} For tunneling in the c direction, the $\Gamma(T)$ dependence near T_c appears to be similar to that predicted by phenomenological marginal-Fermi-liquid theory, in good agreement with a previous report.⁶⁴

D. Ground-state DOS

At low temperature, the data indicate a zero-bias conductance $G_{\text{obs}}(V=0 \text{ mV}, T)/G(V=100 \text{ mV}, T) = 0.15\text{--}0.2$, which is lower than that reported previously for planar junctions.^{25–28} Whether the gapless feature is intrinsic or not has been a matter of argument because the ratio of $N_s(0)/N_n(0)$ is dependent on the choice of the normalization. This uncertainty, however, has been removed in our analysis using the extrapolation of the normal-state conductance. On the other hand, for c -axis tunneling it has been suggested that the condition $G(0) = 0$ occurs only under a particular condition, namely, when the BiO surface is locally nonmetallic or a gap function node appears at the BiO surface.^{65,66} Additionally, in wide-area junctions it cannot be ruled out that a nonzero $G(V=0 \text{ mV}) > 0$ arises from defective nonsuperconducting areas, as has been suggested previously,⁶⁷ or results from an imperfect barrier. In our junction, however, the BiO surface layer of the 2212 single crystal may be considered part of the 2201 layer, which acts either as a barrier layer or a normal-metal layer in a N - S -type junction as discussed above (Fig. 13). In this system, the excess current inside the gap and the zero-bias conductance can

be explained in terms of an Andreev reflection, as discussed above, without background subtraction as used in previous reports. Furthermore, Fig. 10 shows that the shape of gap minimum in $G_{\text{obs}}(V)$ at low temperatures can be fitted by the BCS function including Andreev reflection without lifetime smearing and/or a distribution of gap values. This indicates that the zero-bias conductance is intrinsically quite low or zero. The present results suggest that the order parameter has essentially an s -like symmetry along the c axis, consistent with recent STM tunneling^{13,20,23} and Josephson junction⁶⁸ data, but in conflict with photoemission spectroscopy,⁶⁹ far-infrared spectroscopy,⁷⁰ nuclear-magnetic-resonance,^{71,72} and London-penetration-depth^{73,74} data, which suggest d -wave symmetry. However, since the conductance peak at the gap edge is somewhat broader than that of the BCS curve as shown in Fig. 10, it is possible that a small anisotropy in the order parameter does exist possibly due to an extended s -wave or mixing with d -wave pairing for the superconductivity.

V. CONCLUSION

The temperature-dependent tunneling conductance $G_{\text{obs}}(V, T)$ along the c axis of $\text{Bi}_2\text{Sr}_2\text{CaCu}_2\text{O}_8$ single crystals has been investigated using epitaxial junctions of $\text{Au}/\text{Bi}_2\text{Sr}_2\text{CuO}_6$ thin-film layer/ $\text{Bi}_2\text{Sr}_2\text{CaCu}_2\text{O}_8$ single crystals. The linear background conductance, attributed to a normal density-of-states effect, has been described by

a simple first-order relation with only one fitting parameter. Using this relation, the normal-state background conductance below T_c is obtained by extrapolation from the temperature dependence above T_c . The shape of the superconducting gap structure agrees well with a convolution of this linear background and a BCS density of states modified by Andreev reflection over the entire interval from low temperatures to just below T_c . This fit yields values for the ratio $2\Delta(T=11\text{ K})/k_B T_c$ (84 K) = 5.4–6.0 and a very small lifetime broadening $\Gamma(T=11\text{ K}) < 0.1\text{ meV}$. Both the normal-state background and the superconductive gap structure are consistent with marginal-Fermi-liquid theory without any modification of the BCS density of states. The temperature dependence of the fitted value Δ is consistent with BCS theory. The fits provide a systematic result in which the zero-bias conductance appears intrinsically low or zero, suggesting an s -like character for the electron pairing along the c axis in this system.

ACKNOWLEDGMENTS

We would like to thank K. Kitahama (Institute of Scientific and Industrial Research, Osaka University) for the preparation of the single crystals. We would also like to thank R. Feenstra (Oak Ridge National Laboratory) for useful discussions. This work was supported in part by the Research Aid of the Inoue Foundation for Science and a Grant-in-Aid for Scientific Research from the Ministry of Education, Science and Culture of Japan.

-
- ¹E. L. Wolf, *Principle of Electron Tunneling Spectroscopy* (Oxford University Press, New York, 1985).
²I. Giaever, *Phys. Rev. Lett.* **5**, 147 (1960).
³Q. Huang, J. F. Zasadzinski, N. Tralshawala, K. E. Gray, D. G. Hinks, J. L. Peng, and R. L. Greene, *Nature* **347**, 369 (1990).
⁴J. Z. Zasadzinski, N. Tralshawala, Q. Huang, K. E. Gray, and D. G. Hinks, *IEEE Trans. Magn.* **MAG-27**, 833 (1991).
⁵S. Martin, E. S. Hellman, A. Kussmaul, and E. H. Hartford, Jr., *Phys. Rev. B* **47**, 14 510 (1993).
⁶J. R. Kirtley, *Int. J. Mod. Phys. B* **4**, 201 (1990).
⁷M. Gurvitch, J. M. Valles, Jr., A. M. Cucolo, R. C. Dynes, J. P. Garno, L. F. Schneemeyer, and J. V. Waszczak, *Phys. Rev. Lett.* **63**, 1008 (1989).
⁸A. M. Cucoro, R. C. Dynes, J. M. Valles, Jr., and L. F. Schneemeyer, *Physica C* **179**, 69 (1991).
⁹J. I. Gorina, G. A. Kaljunaia, V. I. Kitorov, V. P. Martovitsky, V. V. Rodin, V. A. Stepanov, A. A. Tsvetkov, and S. I. Vedenev, *Solid State Commun.* **85**, 695 (1993).
¹⁰T. Ekino and J. Akimitsu, *Phys. Rev. B* **40**, 6902 (1989).
¹¹Z. Zhang and C. M. Lieber, *Phys. Rev. B* **47**, 3423 (1993).
¹²Jin-Xiang Liu, S. W. Pierson, G. C. Spalding, Ji-Chun Wan, and A. M. Goldman, *Europhys. Lett.* **20**, 721 (1992).
¹³T. Hasegawa, M. Nantoh, A. Takagi, H. Ikuta, M. Kawasaki, H. Koinuma, and K. Kitazawa, *J. Phys. Chem. Solids* **53**, 1643 (1992).
¹⁴A. M. Cucolo, R. Di Leo, P. Romano, L. F. Schneemeyer, and J. V. Waszczak, *Phys. Rev. B* **44**, 2857 (1991).
¹⁵D. Mandrus, L. Forro, D. Loller, and L. Mihaly, *Nature* **351**, 460 (1991).
¹⁶L. Buschmann, M. Boekholt, and G. Guntherodt, *Physica C* **203**, 68 (1992).
¹⁷R. Escudero, E. Guarner, and F. Morales, *Physica C* **166**, 15 (1990).
¹⁸S. P. Zhao, H. J. Tao, Y. F. Chen, Y. F. Yan, and Q. S. Yang, *Solid State Commun.* **67**, 1179 (1988).
¹⁹Q. Huang, J. F. Zasadzinski, K. E. Gray, J. Z. Liu, and H. Claus, *Phys. Rev. B* **40**, 9366 (1989).
²⁰S. Vieira, J. G. Rodrigo, M. A. Ramos, N. Agrait, K. V. Rao, Y. Makino, and J. L. Costa, *J. Appl. Phys.* **67**, 5026 (1990).
²¹T. Hasegawa, M. Nantoh, and K. Kitazawa, *Jpn. J. Appl. Phys.* **30**, L276 (1991).
²²A. Chang, Zhao Y. Rong, Yu. M. Ivanchenko, Farun Lu, and E. L. Wolf, *Phys. Rev. B* **46**, 5692 (1992).
²³K. Ichimura and K. Nomura, *J. Phys. Soc. Jpn.* **62**, 3661 (1993).
²⁴Jeffrey Kane, Qun Chen, K.-W. Ng, and H.-J. Tao, *Phys. Rev. Lett.* **72**, 128 (1994).
²⁵Mark Lee, D. B. Mitzi, A. Kapitulnik, and M. R. Beasley, *Phys. Rev. B* **39**, 801 (1989).
²⁶E. L. Wolf, H. J. Tao, and B. Susla, *Solid State Commun.* **77**, 519 (1991).
²⁷H. J. Tao, A. Chang, Farun Lu, and E. L. Wolf, *Phys. Rev. B* **45**, 10 622 (1992).
²⁸K. Takahashi, K. Shimaoka, K. Yamano, T. Usuki, Y. Yoshisato, and S. Nakano, *Jpn. J. Appl. Phys.* **31**, 231 (1992).

- ²⁹T. Kawai, T. Matsumoto, M. Kanai, H. Tabata, K. Horiuchi, and S. Kawai, *Physica C* **185-189**, 198 (1991).
- ³⁰T. Matsumoto, T. Kawai, K. Kitahama, S. Kawai, I. Shigaki, and Y. Kawate, *Appl. Phys. Lett.* **58**, 2039 (1991).
- ³¹T. Matsumoto, T. Kawai, K. Kitahama, S. Kawai, I. Shigaki, and Y. Kawate, *Physica C* **185-189**, 1907 (1991).
- ³²T. Matsumoto, T. Kawai, K. Kitahama, and S. Kawai, *Physica C* **198**, 273 (1992).
- ³³I. Shigaki, K. Kitahama, K. Shibutani, S. Hayashi, R. Ogawa, Y. Kawate, T. Kawai, S. Kawai, M. Matsumoto, and J. Shirafuji, *Jpn. J. Appl. Phys.* **29**, L2013 (1990).
- ³⁴M. Tinkham, *Introduction to Superconductivity* (McGraw-Hill, New York, 1975).
- ³⁵A. F. Andreev, *Sov. Phys. JETP* **19**, 1228 (1964).
- ³⁶G. E. Blonder, M. Tinkham, and T. M. Klapwijk, *Phys. Rev. B* **25**, 4515 (1982).
- ³⁷J. R. Kirtley, S. Washburn, and D. J. Scalapino, *Phys. Rev. B* **45**, 336 (1992).
- ³⁸R. C. Dynes, J. P. Garno, B. G. Hertel, and T. P. Orlando, *Phys. Rev. Lett.* **53**, 2437 (1984).
- ³⁹H. R. Zeller and I. Giaever, *Phys. Rev.* **181**, 789 (1969).
- ⁴⁰S. Pan, K. W. Ng, A. L. de Lozanne, J. M. Tarascon, and L. H. Greene, *Phys. Rev. B* **35**, 7220 (1987).
- ⁴¹J. E. Christopher, R. V. Coleman, Acar Isin, and R. C. Morris, *Phys. Rev.* **172**, 485 (1968).
- ⁴²S. L. Cooper, M. V. Klein, B. G. Pazol, J. P. Rice, and D. M. Ginsberg, *Phys. Rev. B* **37**, 5920 (1988).
- ⁴³R. T. Collins, Z. Schlesinger, F. Holtzberg, P. Chaudhari, and C. Feild, *Phys. Rev. B* **39**, 6571 (1989).
- ⁴⁴J. R. Kirtley and D. J. Scalapino, *Phys. Rev. Lett.* **65**, 798 (1990).
- ⁴⁵P. W. Anderson and Z. Zou, *Phys. Rev. Lett.* **60**, 132 (1988).
- ⁴⁶J. C. Phillips, *Phys. Rev. B* **41**, 8968 (1990).
- ⁴⁷P. B. Littlewood and C. M. Varma, *Phys. Rev. B* **45**, 12 636 (1992).
- ⁴⁸K. Tamura, N. Miyakawa, D. Shimada, T. Akahane, and N. Tsuda, *Jpn. J. Appl. Phys.* **31**, L1322 (1992).
- ⁴⁹N. Nagaosa and Patrick A. Lee, *Phys. Rev. Lett.* **64**, 2450 (1990).
- ⁵⁰V. F. Elesin, A. A. Sinchenko, A. A. Ivanov, and S. G. Galkin, *Physica C* **213**, 490 (1993).
- ⁵¹T. Walsh, J. Moreland, R. H. Ono, and T. S. Kalkur, *Phys. Rev. Lett.* **66**, 516 (1991).
- ⁵²A. M. Cucolo, R. Di Leo, A. Nigro, and F. Licci, *Phys. Rev. B* **46**, 9250 (1992).
- ⁵³A. M. Cucolo and R. Di Leo, *Phys. Rev. B* **47**, 2916 (1993).
- ⁵⁴G. E. Blonder and M. Tinkham, *Phys. Rev. B* **27**, 112 (1983).
- ⁵⁵H. Srikanth and A. K. Raychaudhuri, *Phys. Rev. B* **46**, 14 713 (1992).
- ⁵⁶I. Iguchi and Z. Wen, *Physica C* **178**, 1 (1991).
- ⁵⁷T. Kusumori and I. Iguchi, *Jpn. J. Appl. Phys.* **31**, L956 (1992).
- ⁵⁸H. Srikanth, A. K. Raychaudhuri, J. L. Peng, and R. L. Greene, *Physica C* **218**, 245 (1993).
- ⁵⁹P. J. M. van Bentum and H. van Kempen, in *Scanning Tunneling Microscopy I*, edited by H.-J. Guntherodt and R. Wiesendanger (Springer-Verlag, Berlin, 1992).
- ⁶⁰J.S. Tsai, I. Takeuchi, J. Fujita, S. Miura, T. Terashima, Y. Bando, K. Iijima, and K. Yamamoto, *Physica C* **157**, 537 (1989).
- ⁶¹H. Murakami and R. Aoki, *IEICE Trans. Electron* **E76-C**, 1303 (1993).
- ⁶²G. L. Eesley, J. Heremans, M. S. Meyer, G. L. Doll, and S. H. Liou, *Phys. Rev. Lett.* **65**, 3445 (1990).
- ⁶³L. Coffey, *Phys. Rev. Lett.* **64**, 1071 (1990).
- ⁶⁴E. J. Nicol and J. P. Carbotte, *Phys. Rev.* **44**, 7741 (1991).
- ⁶⁵R. A. Klemm and S. H. Liu, *Phys. Rev. B* **44**, 7526 (1991).
- ⁶⁶S. H. Liu and R. A. Klemm, *Phys. Rev. B* **45**, 415 (1992).
- ⁶⁷T. Komeda, G. D. Waddill, P. J. Benning, and J. H. Weaver, *Phys. Rev. B* **43**, 8713 (1991).
- ⁶⁸P. Chaudhari and Shawn-Yu Lin, *Phys. Rev. Lett.* **72**, 1084 (1994).
- ⁶⁹Z.-X. Shen, D. S. Dessau, B. O. Wells, D. M. King, W. E. Spicer, A. J. Arko, D. Marshall, L. W. Lombardo, A. Kapitulnik, P. Dickinson, S. Doniach, J. DiCarlo, A. G. Loeser, and C. H. Park, *Phys. Rev. Lett.* **70**, 1553 (1993).
- ⁷⁰D. Mandrus, Michael C. Martin, C. Kendziora, D. Koller, L. Forro, and L. Mihaly, *Phys. Rev. Lett.* **70**, 2629 (1993).
- ⁷¹N. Bulut and K. J. Scalapino, *Phys. Rev. Lett.* **68**, 706 (1992).
- ⁷²D. Thelen, D. Pines, and Jian Ping Lu, *Phys. Rev. B* **47**, 9151 (1993).
- ⁷³D. A. Bonn, P. Dosanjh, R. Liang, and W. N. Hardy, *Phys. Rev. Lett.* **68**, 2390 (1992).
- ⁷⁴D. A. Bonn, Ruixing Liang, T. M. Riseman, D. J. Baar, D. C. Morgan, Kuan Zhang, P. Dosanjh, T. L. Duty, A. MacFarlane, G. D. Morris, J. H. Brewer, W. N. Hardy, C. Kallin, and A. J. Berlinsky, *Phys. Rev. B* **47**, 11 314 (1993).